Electrocatalysis

DOI: 10.1002/anie.201007859

Platinum Concave Nanocubes with High-Index Facets and Their Enhanced Activity for Oxygen Reduction Reaction**

*Taekyung Yu, Do Youb Kim, Hui Zhang, and Younan Xia**

Platinum nanoparticles are widely used as the primary catalysts in a myriad of industrial processes such as CO/NO_x oxidation in catalytic converters, nitric acid production, petroleum cracking, as well as hydrogen (or alcohol) oxidation and oxygen reduction reactions in fuel-cell technology.[1] For most catalytic reactions, it has been shown that high-index planes, which are associated with large numbers of atomic steps, edges, and kinks hold the key to the enhancement of catalytic performance in terms of activity and/or selectivity. A number of protocols have been demonstrated for generating Pt nanoparticles enclosed by high-index facets, including those based on electrochemical reduction and heat treatment.[2] For example, Sun and co-workers have reported the synthesis of tetrahexahedral (THH) Pt nanocrystals with high-index facets, such as {730}, {210}, and {520}, by applying a square-wave potential to polycrystalline Pt microspheres supported on a glassy carbon electrode.[2a] Although these Pt nanocrystals have been shown to have high catalytic activity, their sizes are still relatively too large and the method of preparation is rather limited in terms of production volume. It still remains a challenge to produce Pt nanocrystals with high-index facets by using a simple, scalable route based on wet chemical reduction.

[*] Dr. T. Yu,[+] D. Y. Kim,[+] Prof. H. Zhang, Prof. Y. Xia
Department of Biomedical Engineering
Washington University
Saint Louis, MO 63130 (USA)
E-mail: xia@biomed.wustl.edu
D. Y. Kim[+]
Department of Chemical and Biomolecular Engineering
(BK21 graduate program)
Korea Advanced Institute of Science and Technology (KAIST)
335 Gwahangro, Yuseong-gu, Daejeon 305-701 (Korea)
Prof. H. Zhang
State Key Laboratory of Silicon Materials and
Department of Materials Science and Engineering
Zhejiang University
Hangzhou, Zhejiang 310027 (People's Republic of China)
[+] These authors contributed equally to this work.

[**] This work was supported in part by the NSF (DMR-0804088) and startup funds from Washington University in St. Louis. Y.X. was also partially supported by the World Class University (WCU) program through the National Research Foundation of Korea funded by the Ministry of Education, Science and Technology (R32-20031). Part of the research was performed at the Nano Research Facility, a member of the National Nanotechnology Infrastructure Network (NNIN), which is supported by the National Science Foundation under award ECS-0335765.

Supporting information for this article is available on the WWW under http://dx.doi.org/10.1002/anie.201007859.

Over the past several years, kinetic control has been demonstrated as a simple and versatile approach to the shape-controlled synthesis of noble-metal nanocrystals in the solution phase. In general, kinetic control can be achieved by: 1) substantially slowing down the formation rate of atoms,[3] 2) using a weak reducing agent,[4] 3) introducing an oxidation process,[5] and 4) taking advantage of Ostwald ripening.[6] When the concentration of metal atoms in the solution is low, the atoms tend to add to the edges and corners of a seed rather than the entire surface, thus leading to the formation of nanocrystals with thermodynamically unfavorable morphologies, including rods, plates, multipods, and dendritic structures.[7]

In recent years, nanocrystals with concave rather than flat faces have attracted attention because of their high-index facets.[8] To this end, Zheng and co-workers have demonstrated the synthesis of concave Pd polyhedral nanocrystals with high electrocatalytic activity for formic acid oxidation.[8a] Mirkin and co-workers have also reported the synthesis of concave cubic Au nanocrystals, and demonstrated higher chemical activity compared to octahedra enclosed by low-index {111} facets.[8b] Herein we report the first synthesis of Pt concave nanocubes enclosed by high-index facets including {510}, {720}, and {830} by slowly adding an aqueous $NaBH_4$ solution and a mixture containing K_2PtCl_4, KBr, and $Na_2H_2P_2O_7$ into deionized water by using two syringe pumps. In this synthesis, the formation of a Pt pyrophosphato complex (that is formed by mixing K_2PtCl_4 and $Na_2H_2P_2O_7$) and the slow addition of this precursor by a syringe pump are believed to play a key role in the formation of Pt concave nanocubes. In this case, the seeds selectively overgrow from corners and edges, and the Br^- ion serves as a capping agent to block the growth of the $\langle 100 \rangle$ axis. The Pt concave nanocubes exhibited substantially enhanced specific activity (per unit surface area) relative to those of Pt nanocubes, cuboctahedra, and commercial Pt/C catalysts that are bounded by low-index facets such as {100} and {111} toward the oxygen reduction reaction (ORR), which is the rate-determining step in a proton-exchange membrane (PCM) fuel cell.

In a typical synthesis, an aqueous $NaBH_4$ solution and a mixture containing K_2PtCl_4, KBr, and $Na_2H_2P_2O_7$ were prepared separately and then injected simultaneously at an injection rate of 67 $\mu L\,min^{-1}$ by using two syringe pumps into deionized water maintained at 95 °C. The color of the solution immediately turned from light pink to black upon the addition of the reactant solutions, thus indicating rapid reduction of $PtCl_4^{2-}$ into elemental Pt by $NaBH_4$. Figure 1a shows a typical transmission electron microscopy (TEM) image of the product that contains Pt nanocubes with a concave structure.

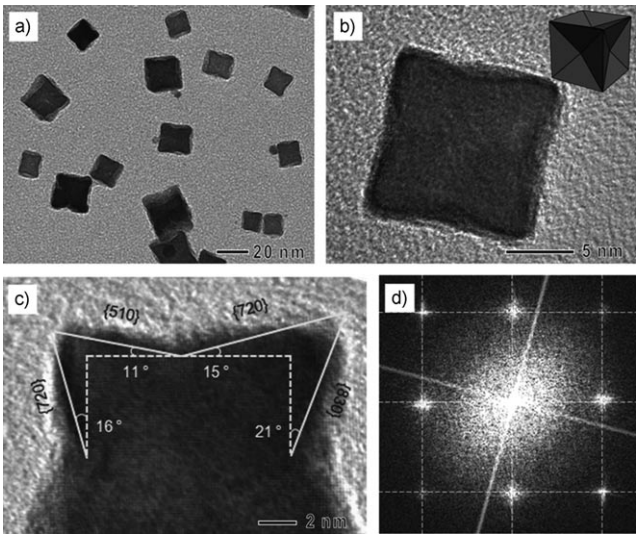

Figure 1. a) TEM and b, c) HRTEM images of Pt concave nanocubes synthesized by continuously adding an aqueous $NaBH_4$ solution and a mixture of K_2PtCl_4, KBr, and $Na_2H_2P_2O_7$ using two syringe pumps into deionized water held at 95 °C. The injection rate was 67 μL min^{-1}, and the KBr/$Na_2H_2P_2O_7$ ratio was 3:1. d) FT pattern of the concave nanocube shown in (c) recorded along the [001] zone axis.

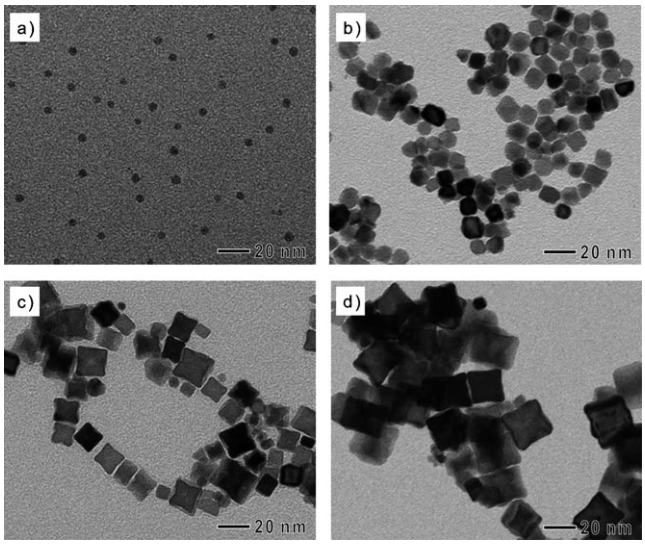

Figure 2. TEM images showing the course of morphological evolution for Pt concave nanocubes. The reaction time was a) 1, b) 3, c) 5, and d) 20 min, respectively.

The edge lengths of the concave nanocubes were in the range of 15–40 nm. Figure 1 b, c, shows high-resolution TEM (HRTEM) images of a single concave nanocube projected along the [100] axis, as confirmed by the corresponding Fourier transform (FT) pattern (Figure 1 d). The angles between the facets of the projected concave nanocube and the {100} facets of an ideal cube were 16°, 11°, 15°, and 21°, which are in agreement with {720}, {510}, {720}, and {830} facets, respectively (Figure 1 c and Figure S1a in the Supporting Information). By measuring the angles of several concave nanocubes, we could conclude that the surface of a Pt concave nanocube was mainly enclosed by {720} facets, together with some other high-index facets such as {510}, {830}, and {310}. A similar structure was recently reported by Mirkin and coworkers for concave nanocubes of Au, the surface of which was enclosed by mostly {720} and some {310} planes.[8b]

To gain an insight into the morphological evolution of the Pt concave nanocubes, aliquots of the reaction solution were removed at various reaction times and examined by TEM. Figure 2 a–d shows typical TEM images of the products sampled at 1, 3, 5, and 20 min, respectively. At $t = 1$ min, the product contained a large number of small Pt nanocrystals with sizes of less than 4 nm (Figure 2 a). In the following 2 min, a number of truncated cubic nanocrystals (ca. 10 nm in size) were observed, thus indicating a rapid growth of the nanocrystals in size (Figure 2 b). As the reaction proceeded to $t = 5$ min, most of Pt nanocrystals exhibited a cubic shape and a concave structure, thus showing a morphological transition from truncated cubes to concave cubes (Figure 2 c). During the next 15 min, the concave cubes further increased in size until they reached edge lengths of 15–40 nm (Figure 2 d). These results indicate that overgrowth of Pt occurred on the seeds along their corners and edges, or the ⟨111⟩ and ⟨110⟩ directions, respectively, thus leading to the formation of a concave structure. The observation of a few small Pt nanoparticles during the growth stage (Figure 2 b–d) suggests the possibility of homogeneous nucleation for the newly formed Pt atoms, even though most of the Pt atoms were preferentially added to the seeds.

In a recent report on the synthesis of Rh nanocrystals, it was demonstrated that manipulating the reaction kinetics could lead to the formation of nanocrystals having anisotropic shapes and/or concave structures.[3c] In the present synthesis, the formation of a complex between K_2PtCl_4 and $Na_2H_2P_2O_7$ and the slow addition of this complex with a syringe pump seem to play the most important role in slowing down the reduction, thus promoting kinetically controlled growth of nanocrystals rather than thermodynamically favored growth. It has been reported that Pt ions can interact with different types of phosphate compounds to form various Pt^{II} or Pt^{IV} phosphato complexes.[9] As shown in the UV/Vis spectra (Figure S2a in the Supporting Information), the absorption peak at 215 nm disappeared after mixing with $Na_2H_2P_2O_7$, thus suggesting that K_2PtCl_4 formed a complex with pyrophosphate ions.[10] The resultant Pt pyrophosphato complex was more difficult to reduce than the initial Pt^{II} ions. On the other hand, when aqueous solutions of $Na_2H_2P_2O_7$ and K_2PtCl_4 were separately prepared and injected into a reaction solution, small Pt nanocrystals with irregular shapes rather than concave nanocubes were observed (Figure S2b). In an effort to obtain a deep understanding of the relationship between the reduction rate and kinetically controlled growth of Pt concave nanocubes, we also conducted the synthesis by rapidly adding solutions of the Pt pyrophosphato complex and $NaBH_4$ with two pipettes instead of syringe pumps, while all other experimental parameters were same as those used to prepare the samples shown in Figure 1. The product was dominated by truncated, nanometer-sized octahedra, which is the thermodynamically favored morphology (Figure S3). The results indicate that a slow reduction rate is vital for kineti-

cally controlled growth, which is a prerequisite for the formation of Pt concave nanocubes.

In addition to the reduction rate, we also systematically investigated the effect of KBr on the morphology of Pt nanocrystals. It has been reported that the selective chemisorption of Br^- ions on the {100} facets of Pt nanocrystals reduces the growth rate along the ⟨100⟩ axis, thus facilitating the formation of nanocubes and nanobars bounded by the {100} facets.[11] To elucidate the role of Br^- ions in controlling the morphology of Pt nanocrystals, we also conducted a set of experiments with different KBr/$Na_2H_2P_2O_7$ molar ratios. When we used only $Na_2H_2P_2O_7$ as a capping agent instead of a KBr/$Na_2H_2P_2O_7$ mixture, the resultant Pt nanocrystals were cuboctahedra enclosed by both {100} and {111} facets (Figure 3a,b). By increasing the amount of KBr, the morphology of Pt nanocrystals exhibited dramatic changes: truncated cubes were formed at a small KBr/$Na_2H_2P_2O_7$ ratio (1:3; Figure 3c,d); cubes at an intermediate ratio of KBr/$Na_2H_2P_2O_7$ (1:1; Figure 3e,f); and concave cubes at a high KBr/$Na_2H_2P_2O_7$ ratio (3:1; Figure 1). These observations demonstrate that reducing the rate of precursor reduction and selective chemisorption of Br^- on {100} facets are both indispensable for the formation of Pt concave nanocubes.

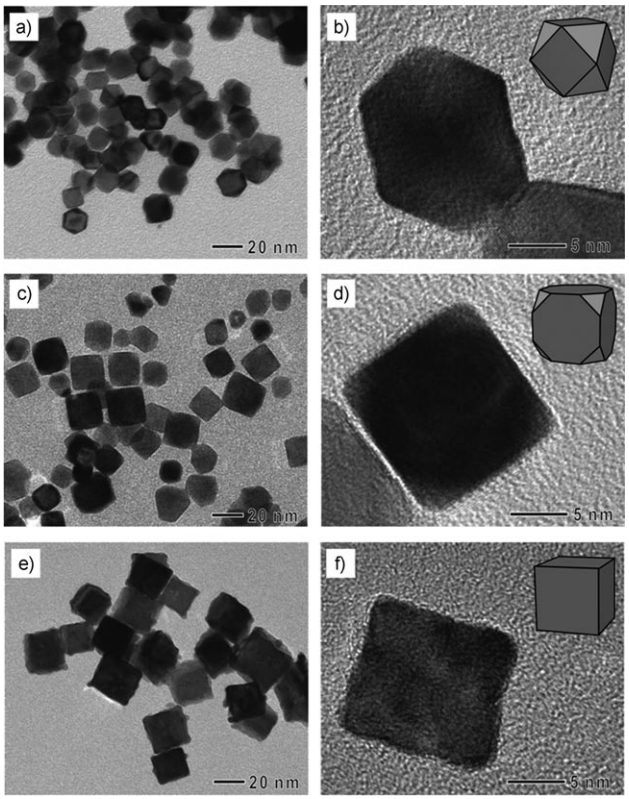

Figure 3. TEM and HRTEM images of a,b) cuboctahedra prepared under the same conditions as in Figure 1 except that the synthesis was conducted in the absence of KBr, c,d) truncated nanocubes prepared under the same conditions as in Figure 1 except that the synthesis was conducted with a low KBr/$Na_2H_2P_2O_7$ ratio (1:3), and e,f) nanocubes prepared under the same conditions as in Figure 1 except that the synthesis was conducted with an intermediate KBr/$Na_2H_2P_2O_7$ ratio (1:1).

The high-index facets of Pt have been shown to have significantly higher ORR activities than their low-index counterparts in acidic solutions.[12] This behavior can be attributed to the favorable adsorption of O_2 molecules onto the stepped surfaces.[13] Cyclic voltammetry (CV) curves recorded at room temperature in a N_2-purged 0.1 mol L^{-1} $HClO_4$ solution with a sweep rate of 50 mV s^{-1} are shown in Figure S4a. The specific electrochemically active surface areas (ECSAs) of Pt nanocrystals were 17.1 $m^2 g_{Pt}^{-1}$ for cuboctahedra, 5.9 $m^2 g_{Pt}^{-1}$ for cubes, and 6.2 $m^2 g_{Pt}^{-1}$ for concave nanocubes, respectively. The Pt cuboctahedra, cubes, and concave cubes were deposited on glassy carbon rotating disk electrodes (RDE) and used for ORR measurements at room temperature in O_2-saturated 0.1 mol L^{-1} $HClO_4$ solutions, with a sweep rate of 10 mV s^{-1} and a rotation rate of 1600 rpm (Figure S4b). To achieve a better understanding of the surface effect between high- and low-index facets, we compared the specific activities (i.e., kinetic current per unit surface area of the nanocatalyst) of these three Pt catalysts. As illustrated in Figure 4a, the specific activity of the Pt concave cubes was 3.1–4.1 and 1.9–2.8 times greater than that of the Pt cubes and cuboctahedra, respectively, in the potential region between 0.8 and 0.95 V, thus demonstrating that the Pt concave cubes exhibited greatly enhanced catalytic activity in the ORR because of its high-index facets. It is worth pointing out that for the low-index facets of Pt, the activity of the ORR increases in the order of

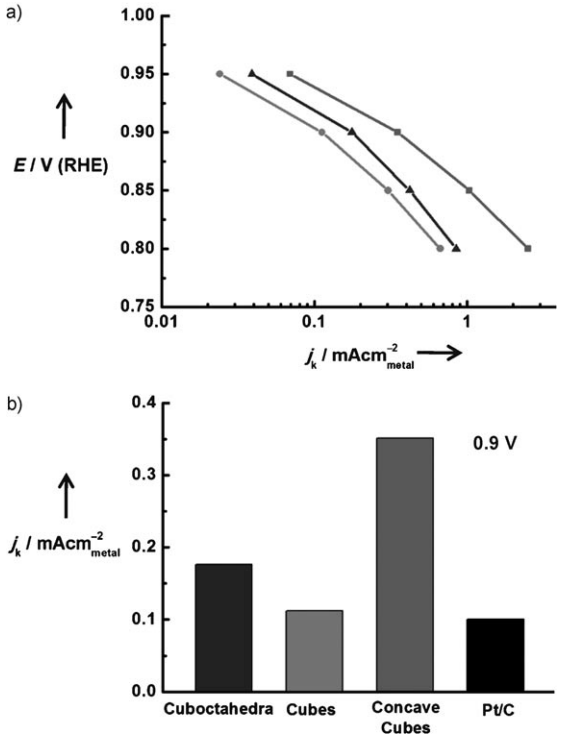

Figure 4. Comparison of the electrocatalytic properties of the Pt concave cubes (■), cubes (●), and cuboctahedra (▲). a) Specific activities given as kinetic current densities (j_k) normalized against the ECSA of the catalyst. b) Specific activities of these catalysts at 0.9 V versus RHE. For all catalysts, the metal loading on the glassy carbon electrode was 15.3 μg cm^{-2}.

(100) and (111) when a non-absorbing electrolyte such as perchloric acid is used.[14] Since Pt cuboctahedra have a mixture of {100} and {111} facets, they are supposed to have a higher ORR activity than Pt cubes enclosed by {100} facets (Figure 4). In comparison with the commercial Pt/C catalyst, the Pt concave cubes exhibited a specific activity that was 3.6 times higher as compared to the 3.2 nm Pt particles on Pt/C catalyst at 0.9 V (Figure 4b). However, the mass activity (i.e., kinetic current per unit Pt mass of catalyst) of Pt concave cubes was still less than that of the Pt/C catalyst, presumably owing to their smaller ECSAs per unit weight of Pt associated with the relatively larger particle size (Figure S5).

In summary, we have demonstrated the synthesis of Pt concave nanocubes enclosed by high-index facets including {510}, {720}, and {830} by using a simple route based on reduction in an aqueous solution. The key to the success of this method is the use of a Pt pyrophosphato complex as the precursor and by controlling the reaction rate with a syringe pump; both facilitate selective overgrowth of seeds from corners and edges, with Br^- serving as a capping agent to block the {100} facets. The Pt concave nanocubes exhibited substantially enhanced electrocatalytic activity per unit surface area towards ORR compared with those of Pt cubes, cuboctahedra, and commercial Pt/C catalysts that are bounded by low-index planes such as {100} and {111}. This work presents another example of kinetic control for generating nanocrystals with high-index facets. We expect that this synthetic strategy could be extended to the synthesis of other noble-metal nanocrystals with high-index facets for highly active catalysts.

Experimental Section

Synthesis of Pt concave nanocubes: In a typical synthesis, a Pt pyrophosphato complex was prepared by adding K_2PtCl_4 (4 mg, 0.01 mmol), $Na_2H_2P_2O_7$ (2 mg, 0.01 mmol), and KBr (6 mg, 0.03 mmol) into deionized water (2 mL). Separately, $NaBH_4$ (0.4 mg) was dissolved in 2 mL deionized water at room temperature. Then, the solutions of the Pt pyrophosphato complex and $NaBH_4$ were continuously added using two syringe pumps at an injection rate of 67 $\mu L\,min^{-1}$ into 3 mL deionized water held at 95 °C under vigorous magnetic stirring. The reaction mixture was left to stand at 95 °C in air for 30 min and then cooled to room temperature. All chemicals were obtained from Aldrich and used as received.

Electrochemical measurements: Electrochemical measurements were performed using a glassy carbon RDE connected to a potentiostat. A hydrogen reference electrode was used, and the counter electrode was a platinum mesh (1 cm × 1 cm) attached to a platinum wire. To prepare the working electrode, the sample was diluted to 0.15 $\mu g\,\mu L^{-1}$ (based on inductively coupled plasma (ICP)-MS measurements) and 20 μL of the dispersion was transferred onto the glassy carbon RDE with a geometric area of 0.196 cm^2. The loading amount of Pt for all catalysts was 3 μg. After evaporation of water, the electrode was coated with 15 μL of 0.05 wt% Nafion solution.

CV measurements were carried out in 0.1 $mol\,L^{-1}$ $HClO_4$ solutions under a flow of N_2 (Airgas, ultrahigh purity) at a sweep rate of 50 $mV\,s^{-1}$. The ECSA was estimated by measuring the charges associated with H_{upd} adsorption/desorption (Q) between 0.05 and 0.40 V after double-layer correction and assuming a value of 210 $\mu C\,cm^{-2}$ for the adsorption of a monolayer of hydrogen onto a Pt surface (q_H). Then, the specific ECSA was calculated based on the following relation: specific ECSA $= 0.5\,Q/(m\,q_H)$, where Q is the charge associated with H_{upd} adsorption or desorption, m is the mass of loaded metal, and q_H is the charge required for the adsorption of a monolayer of hydrogen on a Pt surface.

The ORR measurements were conducted at room temperature in 0.1 M $HClO_4$ solutions under a flow of O_2 (Airgas, Research grade) using the glassy carbon RDE at a rotation rate of 1600 rpm and a sweep rate of 10 $mV\,s^{-1}$. The kinetic current was calculated based on the Koutecky–Levich equation:

$$\frac{1}{i} = \frac{1}{i_k} + \frac{1}{i_d} \quad (1)$$

where i is the experimentally measured current, i_d is the diffusion-limiting current, and i_k is the kinetic current. For each catalyst, the kinetic current was normalized to ECSA in order to obtain specific activities.

Instrumentation: TEM studies were carried out with a FEI Tecnai G2 Spirit microscope operated at 120 kV by drop casting the dispersions of nanoparticles on carbon-coated copper grids. High-resolution TEM analyses were performed using a JEOL 2100F microscope operated at 200 kV accelerating voltage. Both CV and ORR polarization curves were obtained with a PARSTAT 283 poteniostat (Princeton Applied Research). UV/Vis spectra were recorded with a Cary 50 spectrometer (Varian). ICP-MS (ELAN DRC II, Perkin Elmer) was used to determine the amount of Pt catalyst used in each sample for electrochemical measurements.

Received: December 13, 2010
Published online: February 15, 2011

Keywords: electrocatalysis · high-index facets · nanostructures · oxygen reduction reaction · platinum

[1] a) J. Kua, W. A. Goddard, *J. Am. Chem. Soc.* **1999**, *121*, 10928; b) J. Greeley, J. K. Nørskov, M. Mavrikakis, *Annu. Rev. Phys. Chem.* **2002**, *53*, 319; c) X. Wang, M. Waje, Y. Yan, *J. Electrochem. Soc.* **2004**, *151*, A2183; d) J. K. Nørskov, J. Rossmeisl, A. Logadottir, L. Lindqvist, J. R. Kitchin, T. Bligaard, H. Jónsson, *J. Phys. Chem. B* **2004**, *108*, 17886; e) X. Teng, X. Liang, S. Maksimuk, H. Yang, *Small* **2006**, *2*, 249; f) B. Lim, X. Lu, M. Jiang, P. H. C. Camargo, E. C. Cho, E. C. E. Lee, Y. Xia, *Nano Lett.* **2008**, *8*, 4043; g) C. Wang, H. Daimon, T. Onodera, T. Koda, S. Sun, *Angew. Chem.* **2008**, *120*, 3644; *Angew. Chem. Int. Ed.* **2008**, *47*, 3588.

[2] a) N. Tian, Z.-Y. Zhou, S.-G. Sun, Y. Ding, Z. L. Wang, *Science* **2007**, *316*, 732; b) S. W. Lee, S. Chen, W. Sheng, N. Yabuuchi, Y.-T. Kim, T. Mitani, E. Vescovo, Y. Shao-Horn, *J. Am. Chem. Soc.* **2009**, *131*, 15669; c) Z.-Y. Zhou, Z.-Z. Huang, D.-J. Chen, Q. Wang, N. Tian, S.-G. Sun, *Angew. Chem.* **2010**, *122*, 421; *Angew. Chem. Int. Ed.* **2010**, *49*, 411.

[3] a) P.-F. Ho, K.-M. Chi, *Nanotechnology* **2004**, *15*, 1059; b) Y. Xiong, A. R. Siekkinen, J. Wang, Y. Yin, M. J. Kim, Y. Xia, *J. Mater. Chem.* **2007**, *17*, 2600; c) H. Zhang, W. Li, M. Jin, J. Zeng, T. Yu, D. Yang, Y. Xia, *Nano Lett.* **2011**, DOI: 10.1021/nl104347j.

[4] a) I. Washio, Y. Xiong, Y. Yin, Y. Xia, *Adv. Mater.* **2006**, *18*, 1745; b) Y. Xiong, I. Washio, J. Chen, H. Cai, Z.-Y. Li, Y. Xia, *Langmuir* **2006**, *22*, 8563; c) B. Lim, P. H. C. Camargo, Y. Xia, *Langmuir* **2008**, *24*, 10437.

[5] Y. Xiong, J. M. McLellan, J. Chen, Y. Yin, Z.-Y. Li, Y. Xia, *J. Am. Chem. Soc.* **2005**, *127*, 17118.

[6] a) Y. Sun, Y. Xia, *Adv. Mater.* **2003**, *15*, 695; b) Y. Sun, B. Mayers, Y. Xia, *Nano Lett.* **2003**, *3*, 675.

[7] a) J. Park, B. Koo, Y. Hwang, C. Bae, K. An, J.-G. Park, H. M. Park, T. Hyeon, *Angew. Chem.* **2004**, *116*, 2332; *Angew. Chem. Int. Ed.* **2004**, *43*, 2282; b) J. Park, B. Koo, K. Y. Yoon, Y. Hwang,

M. Kang, J.-G. Park, T. Hyeon, *J. Am. Chem. Soc.* **2005**, *127*, 8433; c) B. Koo, J. Park, Y. Kim, S.-H. Choi, Y.-E. Sung, T. Hyeon, *J. Phys. Chem. B* **2006**, *110*, 24318; d) J. Zeng, J. Tao, W. Li, J. Grant, P. Wang, Y. Zhu, Y. Xia, *Chem. Asian. J.* **2010**, **2011**, *6*, 376.

[8] a) X. Huang, S. Tang, H. Zhang, Z. Zhou, N. Zheng, *J. Am. Chem. Soc.* **2009**, *131*, 13916; b) J. Zhang, M. R. Langille, M. L. Personick, K. Zhang, S. Li, C. A. Mirkin, *J. Am. Chem. Soc.* **2010**, *132*, 14012; c) C.-L. Lu, K. S. Prasad, H.-L. Wu, J. A. Ho, M. H. Huang, *J. Am. Chem. Soc.* **2010**, *132*, 14546.

[9] a) R. D. Cornelius, P. A. Hart, W. W. Cleland, *Inorg. Chem.* **1977**, *16*, 2799; b) R. N. Bose, R. E. Viola, R. D. Cornelius, *J. Am. Chem. Soc.* **1984**, *106*, 3336; c) R. J. Mishur, C. Zheng, T. M. Gilbert, R. N. Bose, *Inorg. Chem.* **2008**, *47*, 7972.

[10] L. I. Elding, L. F. Oisson, *J. Phys. Chem.* **1978**, *82*, 69.

[11] a) Y. Xia, Y. Xiong, B. Lim, S. E. Skrabalak, *Angew. Chem.* **2009**, *121*, 62; *Angew. Chem. Int. Ed.* **2009**, *48*, 60; b) B. Lim, M. Jiang, J. Tao, P. H. C. Camargo, Y. Zhu, Y. Xia, *Adv. Funct. Mater.* **2009**, *19*, 189.

[12] a) M. D. Maciá, J. M. Campina, E. Herrero, J. M. Feliu, *J. Electroanal. Chem.* **2004**, *564*, 141; b) A. Kuzume, E. Herrero, J. M. Feliu, *J. Electroanal. Chem.* **2007**, *599*, 333.

[13] a) D. W. Blakely, G. A. Somorjai, *Surf. Sci.* **1977**, *65*, 419; b) N. M. Marković, R. R. Adzic, B. D. Cahan, E. B. Yeager, *J. Electroanal. Chem.* **1997**, *377*, 249.

[14] V. R. Stamenkovic, B. Fowler, B. S. Mun, G. Wang, P. N. Ross, C. A. Lucas, N. M. Marković, *Science* **2007**, *315*, 493.

